

Diamond $\rightarrow\beta$ -tin phase transition in Si within diffusion quantum Monte Carlo

Ryo Maezono

*Japan Advanced Institute of Science and Technology,
School of Information Science, Asahidai 1-1, Nomi, Ishikawa 923-1292, Japan*

N. D. Drummond, A. Ma, and R. J. Needs

*TCM Group, Cavendish Laboratory, University of Cambridge,
J. J. Thomson Avenue, Cambridge CB3 0HE, United Kingdom*

We have studied the diamond $\rightarrow\beta$ -tin phase transition in Si using diffusion quantum Monte Carlo (DMC) methods. Slater-Jastrow-backflow trial wave functions give lower DMC energies than Slater-Jastrow ones, and backflow slightly favors the β -tin phase with respect to the diamond phase. We have investigated the changes in the equation of state that result from the use of different pseudopotentials, the inclusion of either zero-point motion or finite-temperature vibrations, and the application of corrections for finite-size effects. Our tests indicate that the choice of pseudopotential can significantly affect the equation of state. Using a Dirac-Fock pseudopotential leads to an overestimation of the transition pressure but an empirical pseudopotential designed for use in correlated calculations gives a transition pressure in quite good agreement with experiment.

PACS numbers: 02.70.Ss,71.15.Nc,64.60.Ej

I. INTRODUCTION

Calculating accurate energy differences between the atomic structures of materials is one of the central problems in quantum mechanical studies of condensed matter. Here we study the first-order pressure-induced structural phase transition between the diamond and β -tin phases of Si. This is a demanding problem because of the substantial volume change and the increase in the coordination number from four to six at the transition, and the fact that the structural phase transition is accompanied by a metal-insulator transition. Many theoretical studies of the diamond $\rightarrow\beta$ -tin phase transition in Si have been reported, mainly using first-principles density-functional theory (DFT) methods.¹⁻⁸ The DFT results show significant dependence on the density functional used,⁹ indicating the necessity for an accurate description of exchange-correlation effects. A similar dependence on the functional has been noted for self-interstitial defects in Si.⁹⁻¹¹ These results motivate studies using other descriptions of many-body effects such as that provided by quantum Monte Carlo (QMC) methods.

Pressure-induced phase transitions have been studied using the diffusion quantum Monte Carlo (DMC)^{12,13} and auxiliary-field quantum Monte Carlo (AFQMC) methods.¹⁴ The pressure-induced phase transition of Si from the diamond to the β -tin structure has been studied previously using both DMC^{15,16} and AFQMC,¹⁷ while DMC studies of structural phase transitions have also been reported for N₂,¹⁸ MgO,¹⁹ FeO,²⁰ SiO₂,²¹ and BN.²²

The purpose of the present study is to test recent developments in DMC methodology. We have used Slater-Jastrow-backflow (SJB) trial wave functions which go beyond the single-particle nodal surfaces of Slater-Jastrow (SJ) wave functions and significantly lower the energies of the diamond and β -tin phases. We have tested two recent and very different schemes for calculating corrections to the DMC energies obtained with finite supercells that allow us to extrapolate to the infinite-cell limit. To compare the DMC transition pressure and volumes with experiment it is necessary to include the vibrational free energy, which we have re-calculated within DFT with greater accuracy than was achieved in previous studies. Finally we have calculated the energy-volume relations within DFT using different pseudopotentials in order to study the likely influence of the pseudopotential on the DMC transition pressure and volumes and the equations of state of the diamond and β -tin structures.

The rest of the paper is organized as follows. In Sec. II we define the Hamiltonians used and in Sec. III the trial wave functions are described. Finite-size corrections are discussed in Sec. IV and the phonon calculations are described in Sec. V. The main DMC results are reported in Sec. VI. Section VII describes our method for testing different pseudopotentials and reports and discusses results for the equation-of-state parameters and transition pressures and volumes. We draw our conclusions in Sec. VIII. The QMC calculations were performed with the CASINO code,²³ and for the DFT calculations we used the CASTEP plane-wave pseudopotential code.²⁴

II. THE HAMILTONIAN

We used the Dirac-Fock pseudopotential of Trail and Needs²⁵ to describe the interaction of the valence electrons with the Si^{4+} ions. We also added a core-polarization potential (CPP) to each ion.^{26,27} In the CPP approximation, the polarization of each core is determined by the electric field at the nucleus from the instantaneous positions of the electrons and the other atomic cores. CPPs therefore give an approximate description of both dynamical core-valence correlation and static polarization effects. We used the CPP parameters from Ref. 26 and the CPP energy was evaluated using the scheme described in Ref. 28. The non-local pseudopotential energy was calculated using the variational scheme of Ref. 29.

We used 54-atom simulation cells subject to periodic boundary conditions. To make the simulation cell for the diamond structure we took the standard set of primitive translation vectors of the two-atom face-centered-cubic cell and multiplied them by three to give a cell accommodating 54 atoms. The β -tin structure has a body-centered tetragonal lattice and a two-atom primitive unit cell. We used a c/a ratio of 0.556 for the QMC calculations, which is close to the experimental value of 0.5498 reported at the phase transition.³⁰ The energy difference between the structures when using these two c/a ratios is negligible on the scale of interest. The primitive lattice vectors of the two-atom β -tin structure can be chosen to be $\mathbf{u} = (a, a, c)$, $\mathbf{v} = (a, -a, c)$, and $\mathbf{w} = (a, a, -c)$. We wrote a code to search over all possible 54-atom cells constructed from linear combinations of \mathbf{u} , \mathbf{v} , and \mathbf{w} and chose the cell with the maximum value of the shortest distance between supercell lattice points, which has translation vectors \mathbf{U} , \mathbf{V} , and \mathbf{W} , where $\mathbf{U} = -9\mathbf{u} + 3\mathbf{v} + 6\mathbf{w}$, $\mathbf{V} = 3\mathbf{v}$, and $\mathbf{W} = -3\mathbf{u} + 2\mathbf{v} + \mathbf{w}$. Using such a simulation cell gives the largest separation between each electron and its periodic image, which helps to reduce the finite-size effects arising from long-ranged exchange-correlation effects and allows the isotropic terms in the Jastrow factor and backflow transformation (see Sec. III) to give a good description of the electron correlation. The Ewald potential was used to model the interactions between point charges.

III. TRIAL WAVE FUNCTIONS

The DMC method relies on the availability of an accurate trial wave function which is used to guide the sampling and to enforce the fixed-node constraint.^{12,13} We used trial wave functions of SJ and SJB types. The Slater-Jastrow form is

$$\Psi_{\text{SJ}}(\mathbf{R}) = \exp[J(\mathbf{R})] \det \left[\psi_n(\mathbf{r}_i^\uparrow) \right] \det \left[\psi_n(\mathbf{r}_j^\downarrow) \right], \quad (1)$$

where \mathbf{R} denotes the positions of all the electrons, \mathbf{r}_i^\uparrow is the position of the i th spin-up electron, \mathbf{r}_j^\downarrow is the position of the j th spin-down electron, $\exp[J(\mathbf{R})]$ is the Jastrow factor, and $\det \left[\psi_n(\mathbf{r}_i^\uparrow) \right]$ and $\det \left[\psi_n(\mathbf{r}_j^\downarrow) \right]$ are determinants of single-particle orbitals.

The orbitals were calculated using the CASTEP code and a large basis-set energy cutoff of 1088 eV. The orbitals were then transformed into a B-spline or “blip” polynomial basis for greater efficiency.³¹ We used Jastrow factors consisting of polynomial electron-nucleus (en) and electron-electron (ee) terms and a plane-wave ee term,³² with a total of 26 optimizable parameters. We used wave functions both with and without backflow transformations.³³ In the SJB wave function the particle coordinates \mathbf{r}_i in the determinants in Eq. (1) are replaced by collective coordinates

$$\mathbf{x}_i(\mathbf{R}) = \mathbf{r}_i + \boldsymbol{\xi}_i(\mathbf{R}), \quad (2)$$

where $\boldsymbol{\xi}_i(\mathbf{R})$ is the backflow displacement of electron i , which depends on the positions of all of the electrons and ions. The backflow displacement consisted of polynomial ee and en terms³³ and contained a total of 24 optimizable parameters. The wave-function parameters were optimized by a variational Monte Carlo (VMC) procedure in which we first minimized the variance of the energy^{34,35} and then minimized the variational energy itself.³⁶ The wave function parameters were optimized at a single \mathbf{k}_s point in the Brillouin zone of the simulation cell (this being L and M for the diamond and β -tin structures, respectively) and the same Jastrow and backflow parameters were subsequently used for each \mathbf{k}_s point studied, where \mathbf{k}_s is the many-body Bloch vector.³⁷

All of the results reported here were obtained using a DMC time step $\Delta\tau$ of 0.01 a.u. Some test calculations using a SJ trial wave function were also performed with $\Delta\tau = 0.02$ a.u., which give very similar results to those with $\Delta\tau = 0.01$ a.u. We used a target population of 640 configurations in each of our DMC calculations.

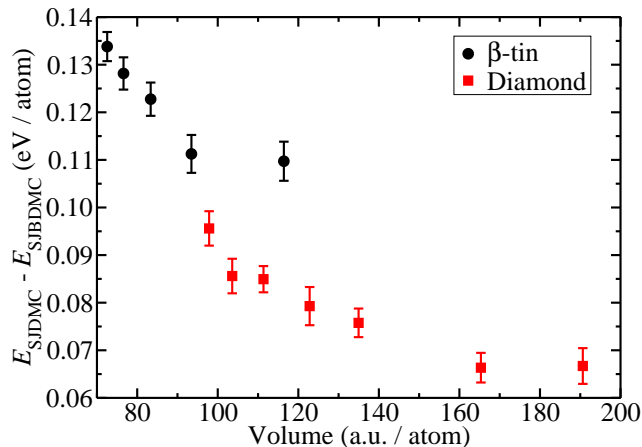


FIG. 1: (Color online) Difference between the SJ and SJB DMC energies for the diamond and β -tin phases. The diamond- and β -tin-structure calculations were performed at the L and M points in the Brillouin zone, respectively.

IV. FINITE-SIZE CORRECTIONS

The 54-atom simulations give a reasonable description of the infinite system, but it is still necessary to make finite-size corrections to obtain accurate results. The finite-size effects can be divided into a part which is very similar to the Brillouin zone integrations performed in single-particle calculations, and exchange-correlation effects arising from electron separations beyond the simulation cell. Brillouin zone integration is more important in metals, where it is required to describe Fermi-surface effects, than in insulators, where a sparse sampling of the Brillouin zone is sufficient. Our 54-atom cells are equivalent to sampling the Brillouin zone of the two-atom primitive cell in a single-particle calculation with 27 \mathbf{k} points.

It is only possible to perform calculations with one simulation-cell Bloch vector \mathbf{k}_s at a time within explicitly correlated methods. For the insulating diamond phase we used only the L -point, which allows the use of a real trial wave function while giving a good description of the energy and charge density in single-particle calculations.^{37,38} For the metallic β -tin phase we performed DMC calculations at twelve randomly chosen \mathbf{k}_s points and averaged the results.³⁹

We tested two different schemes for calculating additional finite-size corrections. In the first scheme we added a further \mathbf{k} -point correction consisting of the difference between the PBE-DFT energies with a very dense \mathbf{k} -point sampling and with the finite \mathbf{k} -point sampling corresponding to that used in the QMC calculations. We then added a correction arising from the long-ranged exchange-correlation interaction using the method described in Refs. 40 and 41, which involves evaluating the static structure factor and two-body Jastrow factor on the grid of reciprocal lattice vectors within QMC and interpolating to obtain an approximate static structure factor and two-body Jastrow factor for the infinite system, from which a finite-size correction can be evaluated. The second scheme is that of Kwee *et al.*⁴² which involves performing a DFT calculation using a modified local density approximation (LDA) functional obtained from DMC calculations for homogeneous electron gases in finite simulation cells subject to periodic boundary conditions. This method includes both the \mathbf{k} -point and long-ranged exchange-correlation corrections, but it also involves making the somewhat stronger assumptions that the LDA is sufficiently accurate and the correction is insensitive to the shape of the simulation cell.

We found excellent agreement between the finite-size corrections obtained from the structure factor method^{40,41} and the DFT method of Kwee *et al.*⁴² The finite-size corrections themselves are quite large, amounting to an increase in energy of about 0.11 eV per atom for the diamond structure and about 0.099 eV per atom for β -tin. However, the difference between the finite-size corrections obtained from the two schemes is, in the worst case, about 0.007 eV per atom, while the average of the absolute deviation over all of the data points for the two structures is 0.004 eV per atom.

V. PHONON CALCULATIONS

We evaluated the phonon contribution to the Helmholtz free energy of each phase as a function of volume using the PBE functional. We used a 64-atom supercell, an energy cutoff of 653 eV, and a $6 \times 6 \times 6$ \mathbf{k} -point mesh to calculate the phonons of the β -tin structure and a 54-atom supercell, a 435 eV cutoff, and a $3 \times 3 \times 3$ \mathbf{k} -point grid for the

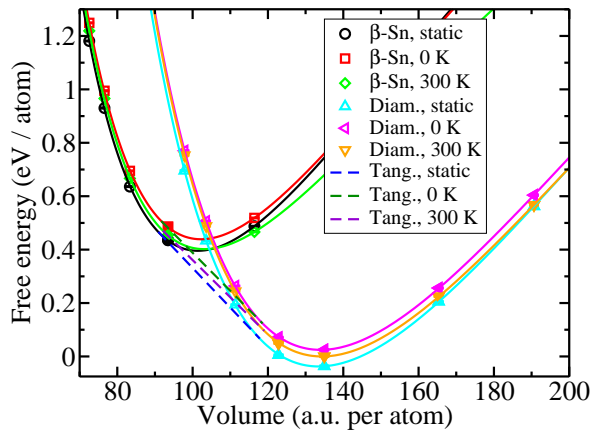


FIG. 2: (Color online) Variation of the free energy with volume for the diamond and β -tin phases of Si calculated within DMC and with corrections for the vibrational energy from PBE-DFT. Static lattice, $T = 0$ and $T = 300$ K results are shown, and the zero of free energy is taken to be the DMC results including vibrational effects at 300 K. The common tangents labeled “Tang.” join the coexistence points. Filled symbols denote that the structures were found to be dynamically stable within the DFT phonon calculations. The statistical error bars on the DMC energies are in the range 0.00005–0.00007 a.u. per atom in all cases.

diamond structure. The phonons frequencies and modes were calculated using a finite-displacement method and the results were extrapolated to zero displacement. Gaál-Nagy *et al.*⁴³ have shown that it is difficult to obtain stable phonon modes of the β -tin phase of Si in DFT calculations. Our study supports this conclusion, and we have found stable phonon modes only by carefully relaxing the c/a ratio at every volume and, even then, the phonon modes are only stable over the volume range 91.4–111.8 a.u. per atom. Over the volume range where the phonons are stable, the variation of the relaxed c/a ratio with volume is well fitted by $c/a = 0.521075 + 0.377765/(131.41 - V)^{0.77666}$, where V is the volume per atom in a.u.

The phonon free energy was calculated from the phonon frequencies. The previous DMC and AFQMC calculations estimated the changes in the transition pressure from nuclear zero-point motion and finite-temperature vibrations using the DFT vibrational data of Gaál-Nagy *et al.*⁴⁴ These data suggest that including zero-point motion reduces the phase transition pressure by about 1 GPa, and that finite-temperature effects at 300 K reduce the transition pressure by a further 0.3 GPa. We believe that Gaál-Nagy *et al.*⁴⁴ have somewhat overestimated the size of the vibrational effects because they used a non-optimal c/a ratio. Our phonon calculations give a reduction in the transition pressure from zero point motion of about 0.62 GPa and a further reduction of 0.34 GPa at 300 K. These values do not differ significantly when we use LDA, PBE, or DMC static-lattice energy-volume curves.

VI. DMC RESULTS

The reduction in the DMC energy resulting from the inclusion of backflow is shown in Fig. 1. The energy reduction is greater in the β -tin phase than in the diamond phase at the same volume, which we conjecture is due to the metallic nature of the β -tin phase. The energy reduction increases with the density of the system, as has been found in studies of the electron gas.⁴⁵ The use of backflow reduces the energies of the diamond structure by 0.07–0.1 eV per atom and the β -tin structure by 0.11–0.13 eV per atom, over the respective volume ranges, but the energy difference between the structures at the transition is reduced by only about 0.015 eV.

The total Helmholtz free energy at temperature T at each volume was evaluated as the sum of the DMC energy, the finite-size correction from the scheme of Kwee *et al.*,⁴² and the phonon free energy. The parameters of the Vinet equation of state⁴⁶ were then calculated using a least-squares fitting procedure. The Helmholtz free energies for the static lattice, zero temperature, and $T = 300$ K cases are shown in Fig. 2. The fitted equation-of-state parameters for the diamond and β -tin structures are given in Tables I and II, respectively, and coexistence pressures, etc., for the phase transition are reported in Table III.

Source	V_0 (a.u. / atom)	B_0 (GPa)	B'_0
Experiment	135.1 ^a	97.9(1) ^b	4.24 ^b
DMC	134.3(1)	97.1(3)	4.18(5)
DMC + BFD-pp	132.3(1)	99.7(3)	4.18(5)
DMC + EMP-pp	133.3(1)	96.2(3)	4.19(5)
DMC + PBE-pp	153.7(1)	85.3(6)	3.67(5)
DMC + LDA-pp	131.4(1)	101.5(3)	4.18(5)
PBE-pp	138.0	86.0	4.52
LDA-pp	132.8	94.4	4.46

^aRef. 47.

^bRef. 48.

TABLE I: The equilibrium volume per atom V_0 , bulk modulus B_0 , and pressure derivative of the bulk modulus B'_0 of diamond-structure Si from experiment and from DMC and DFT calculations. All results are for 300 K.

Source	V_0 (a.u. / atom)	B_0 (GPa)	B'_0
DMC	103.1(1)	102.7(26)	4.7(2)
DMC + BFD-pp	101.4(1)	106.2(26)	4.7(2)
DMC + EMP-pp	102.4(1)	104.2(26)	4.7(2)
DMC + PBE-pp	101.5(1)	105.3(21)	4.7(2)
DMC + LDA-pp	100.6(1)	107.4(21)	4.8(2)
PBE-pp	104.8	94.1	4.74
LDA-pp	103.9	96.0	4.76

TABLE II: The equilibrium volume per atom V_0 , bulk modulus B_0 , and pressure derivative of the bulk modulus B'_0 of β -tin-structure Si from DMC and DFT calculations. All results are for 300 K.

Source	p_t (GPa)	V_{dia} (a.u. / atom)	$V_{\beta\text{-tin}}$ (a.u. / atom)	ΔV_t (a.u. / atom)	ΔF_0 (eV / atom)
Experiment (Ref. 30)	11.7	122.48	94.17	-28.31	-
LDA (This work)	6.17	125.42	95.63	-29.79	0.2681
PBE-GGA (This work)	8.75	126.82	96.95	-29.87	0.2538
DMC (This work)	15.1(1)	119.0(1)	92.1(1)	-26.9(1)	0.405(3)
DMC + BFD-pp (This work)	15.7(1)	117.1(1)	90.5(1)	-26.6(1)	0.418(3)
DMC + EMP-pp (This work)	12.2(1)	120.3(1)	93.2(1)	-27.1(1)	0.329(3)
DMC + PBE-pp (This work)	14.9(1)	134.1(1)	91.0(1)	-43.1(1)	0.656(3)
DMC + LDA-pp (This work)	16.9(1)	115.6(1)	89.3(1)	-26.3(1)	0.446(3)
DMC (Ref. 15)	15.5(5)	-	-	-	-
DMC (Ref. 16)	14(1)	122.4(3)	93.8(7)	-28.69(8)	0.42(2) [†]
AFQMC (Ref. 17)	12.6(3)	122.48*	94.17*	-28.31*	-

TABLE III: The experimental diamond $\rightarrow\beta$ -tin phase transition pressure and volumes and calculated coexistence pressures and volumes in Si, and the difference between the zero-pressure free energies. Volumes are given in a.u. per atom. The asterisks denote that the experimental value was assumed. The data are for $T = 300$ K except for the value marked with a dagger, which is for zero temperature. The addition of a 300 K temperature correction to the value of ΔF_0 from Ref. 16 would result in a decrease of about 0.024 eV per atom.

VII. TESTING DIFFERENT PSEUDOPOTENTIALS

Pseudopotentials are very well established in DFT calculations, where they can give results in excellent agreement with all-electron calculations. The accuracy of pseudopotentials in reproducing all-electron results in explicitly correlated calculations such as QMC is rather more doubtful. One difficulty is that there is no straightforward equivalent of the method normally used within independent electron theories of constructing a pseudopotential by inverting the atomic Schrödinger equation for the valence electrons. Indeed, the idea of dividing the electrons into core and

valence shells is not well defined in the many-body system. The difficulties in generating pseudopotentials which are consistent with correlated methods for calculating the valence electronic structure leads to additional errors.

To examine the DMC results using different pseudopotentials we calculated corrections to the energy-volume curves using different pseudopotentials. We modeled the interactions between the valence electrons by the PBE-GGA functional and approximated the DMC energy for pseudopotential X-pp by

$$\tilde{E}_{\text{DMC}}^{\text{X-pp}} = E_{\text{DMC}}^{\text{DF-pp}} + \left(E_{\text{PBE}}^{\text{X-pp}} - E_{\text{PBE}}^{\text{DF-pp}} \right). \quad (3)$$

where the subscript refers to the method used to calculate the energy, and DF-pp denotes the Dirac-Fock pseudopotential.²⁵ We tested four pseudopotentials: ultrasoft LDA and PBE pseudopotentials, the empirical (EMP) pseudopotential of Ref. 49, and the Hartree-Fock pseudopotential of Burkatzki, Filippi, and Dolg (BFD) from Ref. 50.

There is some evidence that Hartree-Fock (and presumably Dirac-Fock) pseudopotentials give better results within DMC than DFT pseudopotentials.⁵¹ The EMP pseudopotential uses the measured values of the ionization energy of Si^{+3} ions which have a single electron in the $3s$, $3p$, or $3d$ orbital outside of the neon core, and calculated data for the amount of valence charge density outside of the pseudopotential core radius in the ionic states. Corrections for the core relaxation effects arising from generating the pseudopotentials in ionized configurations are also included. Note that Esler *et al.*²² have developed a method for calculating a correction to the QMC energy that accounts for the error due to the pseudopotential approximation. The method uses all-electron results for small systems, although these would be very costly to evaluate for Si.

A. Comparison of equation-of-state parameters

Data for the equilibrium volume V_0 , the bulk modulus B_0 , and the pressure derivative of the bulk modulus B'_0 of diamond-structure Si at 300 K are given in Table I. As shown in numerous DFT calculations, the equilibrium volume V_0 of diamond-structure Si with the PBE functional is larger than experiment while the LDA value is smaller than experiment. The PBE value of B_0 is significantly smaller than experiment while the LDA value is close to experiment, and the PBE and LDA values of B'_0 are rather larger than experiment.^{47,48} The experimental value of B_0 is believed to be very reliable and therefore we can be confident that PBE gives too small a value. Reference 48 does not report an error bar for the measurement of B'_0 and so it may not be safe to draw conclusions about the accuracy of experimental or calculated values for it.

The DMC calculations for the diamond structure with the Dirac-Fock pseudopotential provide very accurate results for V_0 and B_0 . The DMC calculations with corrections for using other pseudopotentials [see Eq. (3)] give results of variable quality. The equation-of-state parameters obtained using the BFD pseudopotential are very similar to those obtained using the Dirac-Fock pseudopotential. This is to be expected because these pseudopotentials were designed to reproduce Hartree-Fock or Dirac-Fock results, and the relativistic effects included in the Dirac-Fock pseudopotential are unimportant for Si. However, the methods used to construct the pseudopotentials are rather different, and it is therefore relevant to compare the results obtained with them. An earlier comparison of the Trail-Needs Dirac-Fock pseudopotentials and the BFD pseudopotentials for the LiH molecule also found that very similar results are obtained with the two classes of pseudopotential.⁵² The equation-of-state parameters obtained with the EMP pseudopotential are close to those from the Dirac-Fock pseudopotential, but the results obtained with the PBE and LDA pseudopotentials are significantly different and are in poorer agreement with experiment. We note that the DMC calculations with the Dirac-Fock, BFD, and EMP pseudopotentials, which give the best values of V_0 and B_0 , also provide the values of B'_0 in the best agreement with experiment (note, however our remark about the lack of an error bar on the experimental value of B'_0). The PBE and LDA pseudopotentials give results which differ substantially from experiment.

The equation-of-state parameters for β -tin-structure Si at 300 K are given in Table II. Experimental data for V_0 , B_0 , and B'_0 are not available for the β -tin structure of Si. We note that the values of V_0 and B'_0 for the β -tin structure are similar for the DMC-based and DFT-based calculations, but the DMC-based calculations give larger values of B_0 .

B. Phase transition pressures and volumes

The best experimental value for the room temperature phase transition pressure is probably that of McMahon and Nelmel of $p_t = 11.7$ GPa,³⁰ which is close to the value of $p_t = 11.3(2)$ GPa found earlier by Hu *et al.*⁵³ Reference 30 also reported the structural parameters of the diamond and β -tin structures at the transition. Several factors should be borne in mind when comparing the experimental and theoretical results. The experimental transition pressure

and volumes were measured on compression while theoretical studies normally report the coexistence pressure, which is expected to be lower because strongly first-order transitions are likely to involve passing over kinetic barriers. Unfortunately the diamond $\rightarrow\beta$ -tin phase transition in Si is irreversible and different structural phases are found on decompression,⁷ so that the coexistence pressure cannot be bracketed by the values obtained on compression and decompression. Prior to compression, the powdered sample is isotropic, but the compression has a uniaxial component and, after the transition, the β -tin phase shows a “preferred orientation”, that is, the microcrystallites have a tendency to align, indicating that the stress on the sample during the transition is anisotropic. Various calculations^{54–57} have shown that an anisotropic stress lowers the transition pressure (the pressure is equal to minus one third of the trace of the stress tensor). As the effects of the anisotropic stress and the kinetic barrier act in opposite directions on the measured transition pressure, and it is difficult to estimate their size, it seems reasonable to neglect them. Finally, the experimental data were measured at room temperature, while the electronic structure calculations were performed at zero temperature and the vibrational effects were added afterwards.

The data in Table III show that the DMC calculations with finite-size and temperature corrections give a coexistence pressure of 15.1(1) GPa, which is 3.4 GPa larger than the measured transition pressure and the DMC calculations underestimate the transition volumes. Correcting the DMC energies to give an approximation to the results that would be obtained using the EMP potential using Eq. (3) gives results for the coexistence pressure and volumes in quite good agreement with the experimental data. Correcting the DMC energies to approximate the results that would be obtained for the PBE and LDA pseudopotentials leads to poorer transition volumes and pressures.

VIII. CONCLUSIONS

Backflow improves the description of exchange-correlation effects and significantly lowers the VMC and DMC energies of the diamond and β -tin phases of Si. These energy reductions, however, mostly cancel in the DMC energy differences between the two phases and, overall, backflow favors the β -tin phase with respect to the diamond phase by roughly 0.015 eV per atom at the transition. In a previous DMC study it was suggested that the overestimation of the experimental transition pressure was most likely to be due to fixed-node errors.¹⁵ The current much-refined study includes backflow transformations which reduce the fixed-node error, but the DMC results with the Dirac-Fock pseudopotential (corrected for finite-size and vibrational effects) are within error bars of the results of Ref. 15. The significant reductions in the energies of the two phases due to the use of backflow make it less likely that the residual errors arise from the fixed-node approximation.

We tested two different schemes designed to correct for the finite sizes of the simulation cells. The finite-size corrections are of order 0.1 eV per atom, but the maximum difference between the corrections provided by the two schemes is only about 0.007 eV per atom. This suggests that both schemes are working extremely well in this system. We calculated the phonon frequencies of the diamond and β -tin phases as a function of volume, finding that it is very important to relax the c/a ratio of the β -tin phase at each volume to obtain stable phonon modes. Even then the β -tin phase was found to be dynamically stable only over a small volume range. Our phonon calculations give a reduction in the transition pressure from including finite-temperature effects at 300 K of nearly 1 GPa, compared with the reduction of 1.3 GPa obtained by Gaál-Nagy *et al.*⁴⁴

Finally, we estimated the DMC results that would be obtained with different pseudopotentials and found a substantial dependence on the pseudopotential. The Dirac-Fock pseudopotential used in our QMC calculations gave a transition pressure of 15.1(1) GPa, while the BFD Hartree-Fock pseudopotential gave very similar results. The EMP pseudopotential gave 12.2(1) GPa, a PBE pseudopotential gave 14.9(1) GPa, and an LDA pseudopotential gave 16.9(1) GPa. The best agreement with experiment was obtained with the EMP pseudopotential. It is worth noting that the EMP pseudopotential is the only one designed for use in explicitly correlated calculations, and that it gave the best results among the Si pseudopotentials tested in correlated calculations in Ref. 49. The values of the equilibrium volume, bulk modulus, and the pressure derivative of the bulk modulus obtained with the EMP pseudopotential were also in good agreement with experiment.

The results of our QMC calculations for Si and, presumably, calculations with other atoms, depend significantly on the pseudopotentials used. We therefore believe that more research is required into the development of pseudopotentials for explicitly correlated methods such as QMC.

Acknowledgments

R.M. acknowledges financial support provided by Precursory Research for Embryonic Science and Technology, Japan Science and Technology Agency (PRESTO-JST), and by a Grant-in-Aid for Scientific Research in Priority

Areas [Development of New Quantum Simulators and Quantum Design (No. 17064016)] (Japanese Ministry of Education, Culture, Sports, Science, and Technology KAKENHI-MEXT). N.D.D. acknowledges financial support from the Leverhulme Trust, Jesus College, Cambridge, and the UK Engineering and Physical Sciences Research Council (EPSRC). R.J.N. acknowledges financial support from EPSRC. We thank John Trail for assistance with the pseudopotentials.

-
- ¹ M. T. Yin and M. L. Cohen, Phys. Rev. B **26**, 5668 (1982).
² R. J. Needs and R. M. Martin, Phys. Rev. B **30**, 5390 (1984).
³ L. L. Boyer, E. Kaxiras, J. L. Feldman, J. Q. Broughton, and M. J. Mehl, Phys. Rev. Lett. **67**, 715 (1991).
⁴ R. J. Needs and A. Mujica, Phys. Rev. B **51**, 9652 (1995).
⁵ N. Moll, M. Bockstedte, M. Fuchs, E. Pehlke, and M. Scheffler, Phys. Rev. B **52**, 2550 (1995).
⁶ K. Gaál-Nagy, M. Schmitt, P. Pavone, and D. Strauch, Comput. Mat. Sci. **22**, 49 (2001).
⁷ A. Mujica, A. Rubio, A. Muñoz, and R. J. Needs, Rev. Mod. Phys. **75**, 863 (2003).
⁸ K. Gaál-Nagy, P. Pavone, and D. Strauch, Phys. Rev. B **69** 134112 (2004).
⁹ E. R. Batista, J. Heyd, R. G. Hennig, B. P. Uberuaga, R. L. Martin, G. E. Scuseria, C. J. Umrigar, and J. W. Wilkins, Phys. Rev. B **74**, 121102 (2006).
¹⁰ W.-K. Leung, R. J. Needs, G. Rajagopal, S. Itoh, and S. Ihara, Phys. Rev. Lett. **83**, 2351 (1999).
¹¹ A. E. Mattsson, R. R. Wixom, and R. Armiento, Phys. Rev. B **77**, 155211 (2008).
¹² D. M. Ceperley and B. J. Alder, Phys. Rev. Lett. **45**, 566 (1980).
¹³ W. M. C. Foulkes, L. Mitas, R. J. Needs, and G. Rajagopal, Rev. Mod. Phys. **73**, 33 (2001).
¹⁴ S. Zhang and H. Krakauer, Phys. Rev. Lett. **90**, 136401 (2003).
¹⁵ D. Alfè, M. J. Gillan, M. D. Towler, and R. J. Needs, Phys. Rev. B **70**, 214102 (2004).
¹⁶ R. G. Hennig, A. Wadehra, K. P. Driver, W. D. Parker, C. J. Umrigar, and J. W. Wilkins, Phys. Rev. B **82**, 014101 (2010).
¹⁷ W. Purwanto, H. Krakauer, and S. W. Zhang, Phys. Rev. B **80**, 214116 (2009).
¹⁸ L. Mitas and R. M. Martin, Phys. Rev. Lett. **72**, 2438 (1994).
¹⁹ D. Alfè, M. Alfredsson, J. Brodholt, M. J. Gillan, M. D. Towler, and R. J. Needs, Phys. Rev. B **72**, 014114 (2005).
²⁰ J. Kolorenc and L. Mitas, Phys. Rev. Lett. **101**, 185502 (2008).
²¹ K. P. Driver, R. E. Cohen, Z. Wu, B. Militzer, P. López Ríos, M. D. Towler, R. J. Needs, and J. W. Wilkins, Proc. Natl. Acad. Sci. USA **107**, 9519 (2010).
²² K. P. Esler, R. E. Cohen, B. Militzer, J. Kim, R. J. Needs, and M. D. Towler, Phys. Rev. Lett. **104**, 185702, (2010).
²³ R. J. Needs, M. D. Towler, N. D. Drummond, and P. López Ríos, J. Phys.: Condens. Matter **22**, 023201 (2010).
²⁴ S. J. Clark, M. D. Segall, C. J. Pickard, P. J. Hasnip, M. I. J. Probert, K. Refson, and M. C. Payne, Z. Kristallogr. **220**, 567 (2005).
²⁵ J. R. Trail and R. J. Needs, J. Chem. Phys. **122**, 014112 (2005); J. R. Trail and R. J. Needs, J. Chem. Phys. **122**, 174109 (2005); see also www.tcm.phy.cam.ac.uk/~mdt26/casino2_pseudopotentials.html.
²⁶ E. L. Shirley and R. M. Martin, Phys. Rev. B **47**, 15413 (1993).
²⁷ Y. Lee and R. J. Needs, Phys. Rev. B **67**, 035121 (2003).
²⁸ R. Maezono, M. D. Towler, Y. Lee, R. J. Needs, Phys. Rev. B **68**, 165103 (2003).
²⁹ M. Casula, Phys. Rev. B **74**, 161102 (2006).
³⁰ M. I. McMahon, R. J. Nelmes, N. G. Wright, and D. R. Allan, Phys. Rev. B **50**, 739 (1994).
³¹ D. Alfè and M. J. Gillan, Phys. Rev. B **70**, 161101 (2004).
³² N. D. Drummond, M. D. Towler, and R. J. Needs, Phys. Rev. B **70**, 235119 (2004).
³³ P. López Ríos, A. Ma, N. D. Drummond, M. D. Towler, and R. J. Needs, Phys. Rev. E **74**, 066701 (2006).
³⁴ C. J. Umrigar, K. G. Wilson, and J. W. Wilkins, Phys. Rev. Lett. **60**, 1719 (1988).
³⁵ N. D. Drummond and R. J. Needs, Phys. Rev. B **72**, 085124 (2005).
³⁶ C. J. Umrigar, J. Toulouse, C. Filippi, S. Sorella, and R. G. Hennig, Phys. Rev. Lett. **98**, 110201 (2007).
³⁷ G. Rajagopal, R. J. Needs, S. Kenny, W. M. C. Foulkes, and A. James, Phys. Rev. Lett. **73**, 1959 (1994); G. Rajagopal, R. J. Needs, A. James, S. D. Kenny, and W. M. C. Foulkes, Phys. Rev. B **51**, 10591 (1995).
³⁸ P. R. C. Kent, R. Q. Hood, A. J. Williamson, R. J. Needs, W. M. C. Foulkes, and G. Rajagopal, Phys. Rev. B **59**, 1917 (1999).
³⁹ C. Lin, F. H. Zong, and D. M. Ceperley, Phys. Rev. E **64**, 016702 (2001).
⁴⁰ S. Chiesa, D. M. Ceperley, R. M. Martin, and M. Holzmann, Phys. Rev. Lett. **97**, 076404 (2006).
⁴¹ N. D. Drummond, R. J. Needs, A. Sorouri, and W. M. C. Foulkes, Phys. Rev. B **78**, 125106 (2008).
⁴² H. Kwee, S. Zhang, and H. Krakauer, Phys. Rev. Lett. **100**, 126404 (2008). A related idea was introduced by M. Nekovee, W. M. C. Foulkes, and R. J. Needs, Phys. Rev. Lett. **87**, 036401 (2001); *ibid.* Phys. Rev. B **68**, 235108 (2003).
⁴³ K. Gaál-Nagy, Phys. Rev. B **77**, 024309 (2008).
⁴⁴ K. Gaál-Nagy, A. Bauer, M. Schmitt, K. Karch, P. Pavone, and D. Strauch, Phys. Stat. Sol. B **211**, 275 (1999).
⁴⁵ Y. Kwon, D. M. Ceperley, and R. M. Martin Phys. Rev. B **58**, 6800 (1998).
⁴⁶ P. Vinet, J. Ferrante, J. R. Smith, and J. H. Rose, J. Phys. C: Solid State Phys. **19**, L467 (1986).
⁴⁷ D. Windisch and P. Becker, Phys. Status Solidi (a) **118**, 379 (1990).

- ⁴⁸ H. J. McSkimin and P. Andreatch, Jr., *J. Appl. Phys.* **35**, 2161 (1964).
- ⁴⁹ Y. Lee, P. R. C. Kent, M. D. Towler, R. J. Needs, and G. Rajagopal, *Phys. Rev. B* **62**, 13347 (2000). The parameters of the empirical Si pseudopotential are available from the authors.
- ⁵⁰ M. Burkatzki, C. Filippi, and M. Dolg, *J. Chem. Phys.* **126**, 234105 (2007).
- ⁵¹ C. W. Greeff and W. A. Lester, Jr., *J. Chem. Phys.* **109**, 1607 (1998).
- ⁵² J. R. Trail and R. J. Needs, *J. Chem. Phys.* **128**, 204103 (2008).
- ⁵³ J. Z. Hu, L. D. Merkle, C. S. Menoni, and I. L. Spain, *Phys. Rev. B* **34**, 4679 (1986).
- ⁵⁴ H. Libotte and J. P. Gaspard, *Phys. Rev. B* **62**, 7110 (2000).
- ⁵⁵ C. Cheng, *Phys. Rev. B* **67**, 134109 (2003).
- ⁵⁶ K. Gaál-Nagy and D. Strauch, *Phys. Rev. B* **73**, 134101 (2006).
- ⁵⁷ M. Durandurdu, *J. Phys.: Condens. Matter* **20**, 325232 (2008).